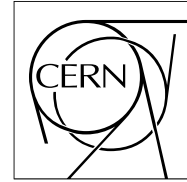


The Compact Muon Solenoid Experiment

CMS Performance Note

Mailing address: CMS CERN, CH-1211 GENEVA 23, Switzerland



10 August 2015

Alignment of the CMS Tracking-Detector with First 2015 Cosmic-Ray and Collision Data

The CMS Collaboration

Abstract

The performance of the CMS tracking-detector alignment with the first 2015 cosmic-ray data and proton-proton collision data at 13 TeV center-of-mass energy with the magnetic field at 0 T and 3.8 T is presented.

Alignment of the CMS Tracking-Detector with First 2015 Cosmic-Ray and Collision Data

The CMS Collaboration

`cms-dpg-conveners-tracker@cern.ch`

2015

Introduction

Distinct data-taking periods in 2015 considered here: cosmic-ray data with the magnetic field at 0 T and 3.8 T prior to the LHC collision-data operation, 0 T collision data at 13 TeV center-of-mass energy, and 3.8 T collision data at 13 TeV center-of-mass energy. During the collision-data periods, also cosmic-ray data has been taken in-between fills of the LHC ('interfill cosmics'). The data-taking periods correspond to different detector geometries, particularly due to changes of the magnetic field. Alignment constants have been derived for each data-taking period using the data collected during that period.

Alignments under study are the result of a combination of a global (Millepede-II) [1, 2] and local (HIP) [2] fit approach. The results are obtained by different approaches of running the two algorithms in sequence. In each data-taking period, the starting point for the alignment fit is the alignment obtained in the previous data-taking period. In addition, the two algorithms run independently confirm each other.

The CMS tracking detector system and the coordinate systems (both the primed and non-primed coordinates) used in the following are defined in [1, 2]. The track reconstruction is described in [3].

The pixel subdetector modules in one half-barrel were repaired during the shutdown, and the pixel subdetectors were also re-centered around the beampipe by $(-1.3, -3.38)$ mm in (x, y) .

Outline

1 Tracker-Geometry Comparisons

- Run II vs Run I Geometries
- Effect of B-Field Changes

2 DMR Validation

- 3.8 T Cosmic-Ray Data
- 0 T Collision Data
- 3.8 T Collision Data

3 Cosmic-Track Splitting Validation

- 3.8 T Cosmic-Ray Data
- 0 T Cosmic-Ray Data

4 Primary-Vertex Validation

- Run II only alignments
- Including Run I alignment

Run II vs Run I Pixel-Detector Geometries

CMS Preliminary

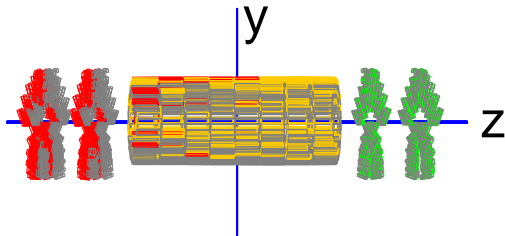
Alignment: cosmic rays + 0T collisions

Run II vs. Run I geometry, shift x 5

> 4 mm

2 mm - 4 mm

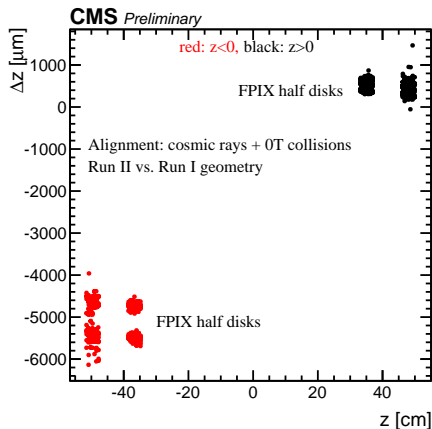
< 2 mm



Also as ANIMATED GIF

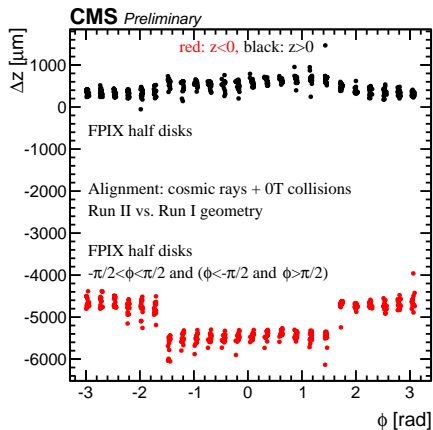
Comparison of Run II and Run I positions of the pixel modules of the tracker, determined with the Millepede-II and HIP algorithms using cosmic ray data collected with 0 T and 3.8 T magnetic field in the solenoid and 0 T collision data at 13 TeV. The positions at the end of Run I are shown in gray. The module shifts (absolute shifts in (x,y,z)) between Run I and Run II are magnified by a factor of 5 for visualization, and the resulting positions are shown in red, yellow, or green, depending on the magnitude of the shift. The red is mostly concentrated in the $-z$ endcap, which moved by about 6 mm away from the barrel. The barrel is mostly yellow, as it was moved up by $(-1.3,-3.38)$ mm in (x,y) in the re-centering procedure around the beampipe during the installation phase prior to Run II. Because of additional movements of the two half-barrels, a few modules are red. The half barrel on the $+x$ side (direction inwards into the picture) was in addition subject of extensive repair and replacement work.

Run II vs Run I FPIX Detector Geometries (Δz vs z)



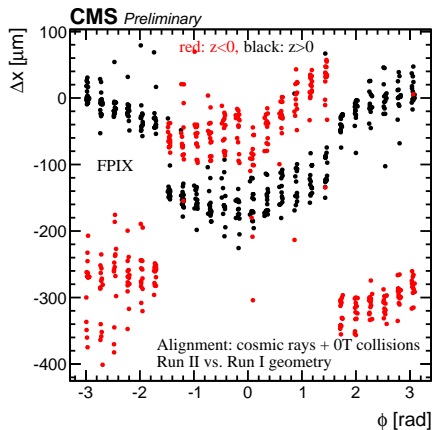
Comparison of Run II and Run I positions of the modules in the forward-pixel (FPIX) detector of the tracker, determined with the Millepede-II and HIP algorithms using cosmic ray data collected with 0 T and 3.8 T magnetic field in the solenoid and 0 T collision data at 13 TeV. Shown is the difference $\Delta z(\text{Run II} - \text{Run I})$ as a function of z in global coordinates. Modules in the endcap half-disks at the $-z$ side are shown in red, modules in the half-disks at the $+z$ side are shown in black. The four half-disks at the $-z$ side (four clusters of red dots) are displaced by -4.5 mm and -5.5 mm. Much smaller relative movements of up to $200 \mu\text{m}$ are observed for the modules in the half-disks on the $+z$ side (two clusters of black dots).

Run II vs Run I FPIX Detector Geometries (Δz vs ϕ)



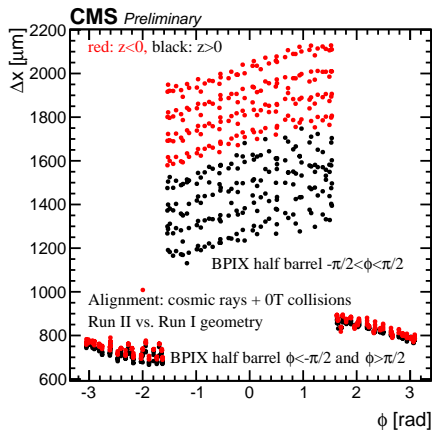
Comparison of the Run II and Run I positions of the modules in the forward-pixel (FPIX) detector of the tracker, determined with the Millepede-II and HIP algorithms using cosmic ray data collected with 0 T and 3.8 T magnetic field in the solenoid and 0 T collision data at 13 TeV. Shown is the difference $\Delta z(\text{Run II} - \text{Run I})$ as a function of ϕ in global coordinates. Modules in the endcap half-disks at the $-z$ side are shown in red, modules in the half-disks at the $+z$ side are shown in black. The half-disks at the $-z$ side are displaced by -4.5 mm ($\phi < -\pi/2$, $\phi > \pi/2$) and -5.5 mm ($-\pi/2 < \phi < \pi/2$) compared to the Run I position. Much smaller relative movements of up to $200 \mu\text{m}$ are observed between the half-disks on the $+z$ side.

Run II vs Run I FPIX Detector Geometries (Δx vs ϕ)



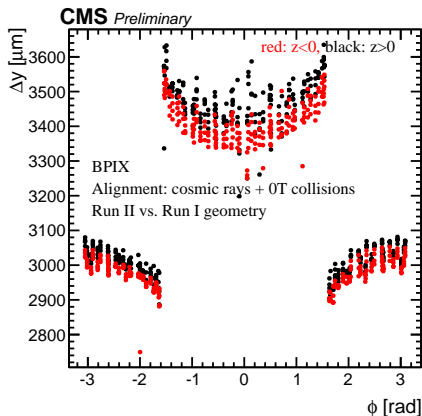
Comparison of Run II and Run I positions of the modules in the forward-pixel (FPIX) detector of the tracker, determined with the Millepede-II and HIP algorithms using cosmic ray data collected with 0 T and 3.8 T magnetic field in the solenoid and 0 T collision data at 13 TeV. Shown is the difference Δx (Run II - Run I) as a function of ϕ in global coordinates. Modules in the endcap half-disks at the $-z$ side are shown in red, modules in the half-disks at the $+z$ side are shown in black. Relative movements between the half-disk structures $-\pi/2 < \phi < \pi/2$ and $\phi < -\pi/2$, $\phi > \pi/2$ are visible, which are more pronounced up to $300 \mu\text{m}$ at the $-z$ side.

Run II vs Run I BPIX Detector Geometries (Δx vs ϕ)



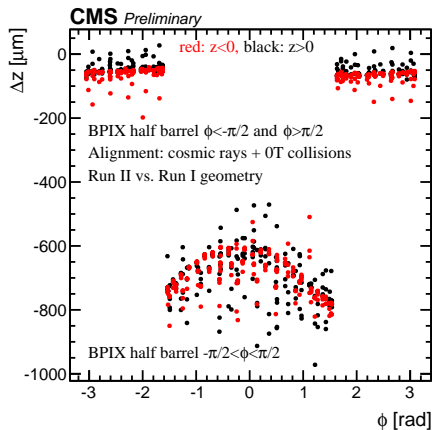
Comparison of Run II and Run I positions of the modules in the barrel-pixel (BPIX) detector of the tracker, determined with the Millepede-II and HIP algorithms using cosmic ray data collected with 0 T and 3.8 T magnetic field in the solenoid and 0 T collision data at 13 TeV. Shown is the difference Δx (Run II - Run I) as a function of ϕ in global coordinates. The BPIX as a whole is subject to a ≈ 2 mm shift attributed to the shifts (-1.3, -3.38) mm introduced in (x,y) in the re-centering procedure of the BPIX around the beampipe during the installation phase. In addition, a relative movement between the two half-barrel structures $-\pi/2 < \phi < \pi/2$ and $\phi < -\pi/2$, $\phi > \pi/2$ is visible, and the individual modules in the half-barrel structure $-\pi/2 < \phi < \pi/2$ move within a range of up to 1 mm. Also, the z-dependence of the spread in x shows that there is a tilt of one half-barrel. This is attributed to the extensive repair and replacement work of this half barrel.

Run II vs Run I BPIX Detector Geometries (Δy vs ϕ)



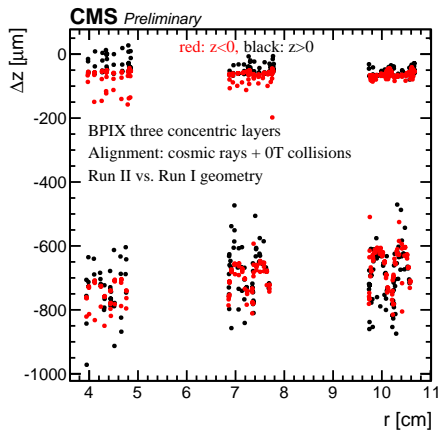
Comparison of Run II and Run I positions of the modules in the barrel-pixel (BPIX) detector of the tracker, determined with the Millepede-II and HIP algorithms using cosmic ray data collected with 0 T and 3.8 T magnetic field in the solenoid and 0 T collision data at 13 TeV. Shown is the difference Δy (Run II - Run I) as a function of ϕ in global coordinates. The BPIX as a whole is subject to a 3-3.5 mm shift attributed to the shifts (-1.3,-3.38) mm introduced in (x,y) the re-centering procedure of the BPIX around the beampipe during the installation phase. In addition, a relative shift between the two half-barrel structures $-\pi/2 < \phi < \pi/2$ and $\phi < -\pi/2$, $\phi > \pi/2$ is visible, which is attributed to the extensive repair and replacement work in the $-\pi/2 < \phi < \pi/2$ half barrel.

Run II vs Run I BPIX Detector Geometries (Δz vs ϕ)



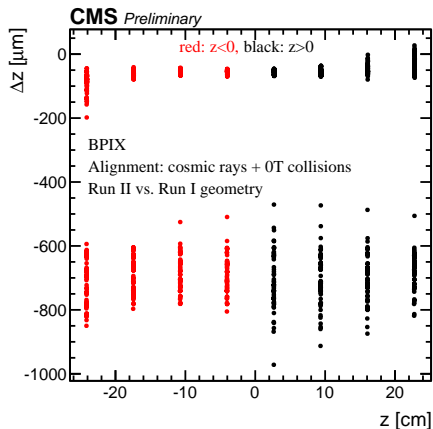
Comparison of Run II and Run I positions of the modules in the barrel-pixel (BPIX) detector of the tracker, determined with the Millepede-II and HIP algorithms using cosmic ray data collected with 0 T and 3.8 T magnetic field in the solenoid and 0 T collision data at 13 TeV. Shown is the difference Δz (Run II - Run I) as a function of ϕ in global coordinates. A relative movement of $\approx 700 \mu\text{m}$ between the two half-barrel structures $-\pi/2 < \phi < \pi/2$ and $\phi < -\pi/2, \phi > \pi/2$ is visible, and the individual modules in the half-barrel structure $-\pi/2 < \phi < \pi/2$ move within a range of $\approx 200 \mu\text{m}$. This is attributed to the extensive repair and replacement work of this half barrel.

Run II vs Run I BPIX Detector Geometries (Δz vs r)



Comparison of Run II and Run I positions of the modules in the barrel-pixel (BPIX) detector of the tracker, determined with the Millepede-II and HIP algorithms using cosmic ray data collected with 0 T and 3.8 T magnetic field in the solenoid and 0 T collision data at 13 TeV. Shown is the difference Δz (Run II - Run I) as a function of the radius r in global coordinates. Six clusters of modules are visible. Clusters around the same three values of r correspond to modules in the three concentric layers of the two BPIX half-barrels. In each layer (at each of the three values of r) two clusters are visible, one close to $\Delta z = 0$ and one cluster of modules with movements of $\approx 700 \mu\text{m}$, indicating a movement of one half-barrel.

Run II vs Run I BPIX Detector Geometries (Δz vs z)



Comparison of Run II and Run I positions of the modules in the barrel-pixel (BPIX) detector of the tracker, determined with the Millepede-II and HIP algorithms using cosmic ray data collected with 0 T and 3.8 T magnetic field in the solenoid and 0 T collision data at 13 TeV. Shown is the difference $\Delta z(\text{Run II} - \text{Run I})$ as a function of z in global coordinates. Modules in the lower part of the plot, corresponding to one half barrel, have moved about $700 \mu\text{m}$, while the other half barrel does not show movements of this size.

Effect of B-Field Changes on Pixel-Detector Geometry

CMS Preliminary

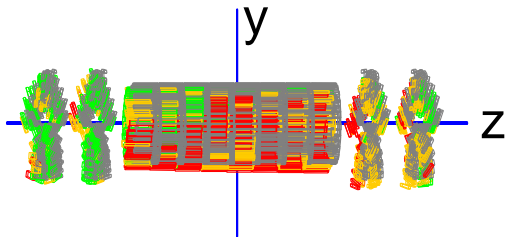
Alignment: cosmic rays

3.8T vs. 0T Run II geometry, shift x 200

> 150 μm

100 μm - 150 μm

< 100 μm



Also as ANIMATED GIF

Comparison of the 3.8 T position of the pixel modules of the tracker to their 0 T position, determined with the Millepede-II and HIP algorithms using 0 T and 3.8 T cosmic ray data. The positions during the first 0 T cosmic ray data collection are shown in gray. The module shifts (absolute shift in (x,y,z)), which resulted from the changing magnetic field, are magnified by a factor of 200 for visualization, and the resulting positions are shown in red, yellow, or green, depending on the magnitude of the shift. The movements are of order 100 μm , and the largest movements are found in the barrel.

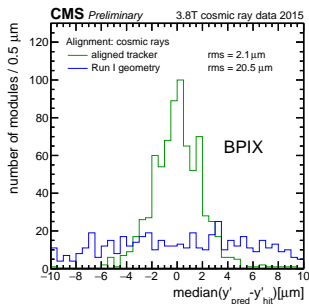
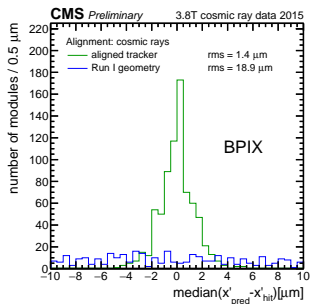
DMR Validation

Distributions of medians of unbiased track-hit residuals. Each track is refitted using the alignment constants under consideration, and the hit prediction for each module is obtained from all of the other track hits. The median of the distribution of unbiased hit residuals is then taken for each module and is histogrammed. The width of this distribution of the medians of residuals (DMR) is a measure of the statistical precision of alignment results; deviations from zero indicate possible biases. The width also has an intrinsic component due to the limited number of tracks, meaning that distributions can only be compared if they are produced with the same number of tracks, as is the case within each set of plots here.

3.8 T Cosmic-Ray Data

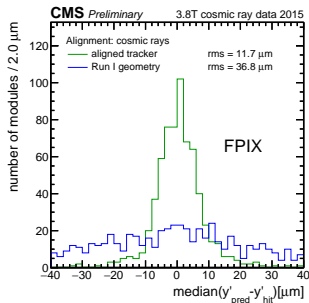
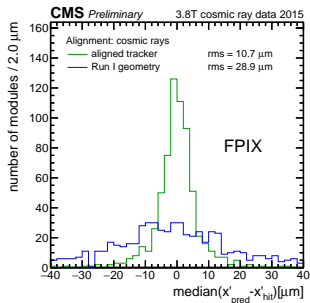
The first alignment of the tracker, using 0 T and 3.8 T cosmic ray data, corrected for the shifts that took place since the end of Run I of the LHC. This validation was performed with 2 million cosmic tracks recorded with a magnetic field of 3.8 T. Large improvements over the Run I geometry are observed in both the pixel (BPIX and FPIX) and the strip (TIB, TID, TOB, TEC) modules. Although the strips moved much less than the pixels did, the pixel misalignment results in less accurate tracks, with effects that are visible in the strips as well.

3.8 T Cosmic-Ray Data: BPIX



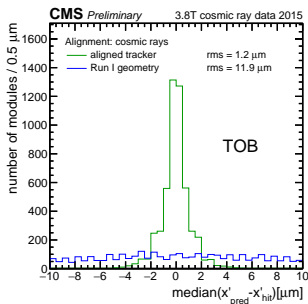
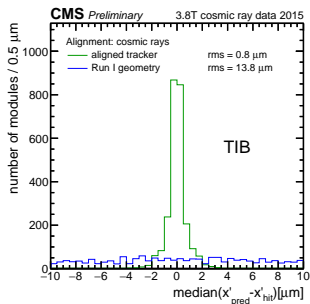
The distribution of median residuals is plotted for the local x - and y -directions in the barrel pixel detector, using 2 million cosmic ray tracks collected with the magnetic field at 3.8 T. The blue line shows the Run I geometry, which is no longer valid for Run II data, primarily because of temperature changes and pixel re-centering and repair. The alignment shown in green was produced with the Millepede-II and HIP algorithms using 0 T and 3.8 T cosmic ray data. The rms values, calculated using modules both inside and outside the plot range, show improvement over the Run I geometry by a factor of 10.

3.8 T Cosmic-Ray Data: FPIX



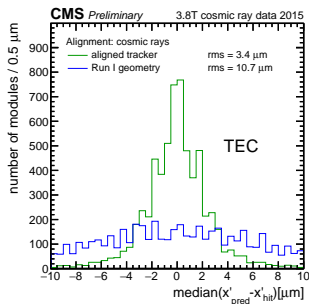
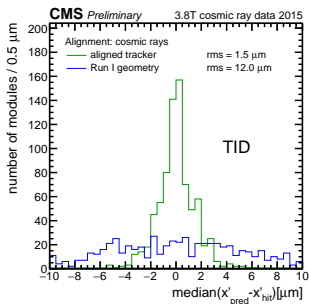
The distribution of median residuals is plotted for the local x - and y -direction in the forward pixel detectors, using 2 million cosmic ray tracks collected with the magnetic field at 3.8 T. The blue line shows the Run I geometry, which is no longer valid for Run II data, primarily because of temperature changes and pixel re-centering and repair. The alignment shown in green was produced with the Millepede-II and HIP algorithms using 0 T and 3.8 T cosmic ray data. The rms values, calculated using modules both inside and outside the plot range, show improvement over the Run I geometry by a factor of 3.

3.8 T Cosmic-Ray Data: TIB and TOB



The distribution of median residuals is plotted for the tracker inner and outer barrel, using 2 million cosmic ray tracks collected with the magnetic field at 3.8 T. The blue line shows the Run I geometry, which is no longer valid for Run II data, primarily because of temperature changes and pixel re-centering and repair (since tracks are fitted using hits in both the pixel and the strip detectors, the large movements of the pixel detectors also affect the DMR performance in the strip detectors). The alignment shown in green was produced with the Millepede-II and HIP algorithms using 0 T and 3.8 T cosmic ray data. The rms values, calculated using modules both inside and outside the plot range, show improvement over the Run I geometry by a factor of 10.

3.8 T Cosmic-Ray Data: TID and TEC

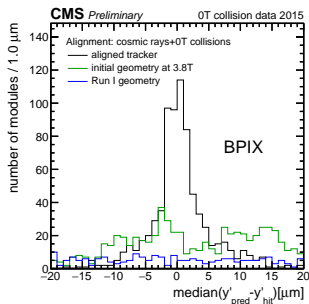
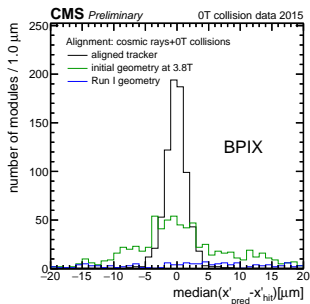


The distribution of median residuals is plotted for the tracker inner disks and endcaps, using 2 million cosmic ray tracks collected with the magnetic field at 3.8 T. The blue line shows the Run I geometry, which is no longer valid for Run II data, primarily because of temperature changes and pixel re-centering and repair (since tracks are fitted using hits in both the pixel and the strip detectors, the large movements of the pixel detectors also affect the DMR performance in the strip detectors). The alignment shown in green was produced with the Millepede-II and HIP algorithms using 0 T and 3.8 T cosmic ray data. The rms values, calculated using modules both inside and outside the plot range, show improvement over the Run I geometry by a factor of 10 (TID) and 3 (TEC).

0 T Collision Data

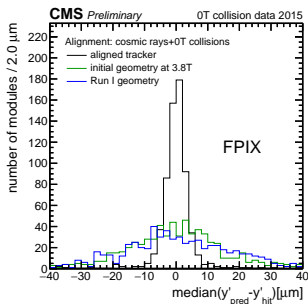
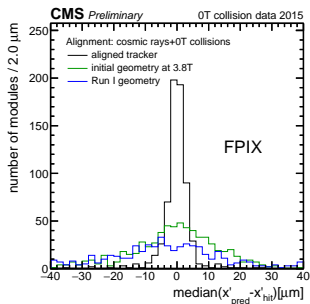
The tracker geometry changed between the 3.8 T cosmic ray data and the first collisions, recorded with the magnetic field off, primarily because the changing magnetic field causes movements in the tracker. These effects are apparent mostly in the pixels, and the alignment performed using 0 T collisions and cosmic rays (taken in between collision-data runs) recovers the tracker performance. These plots are produced with 1.8 million 0 T collision-data tracks.

0 T Collision Data: BPIX



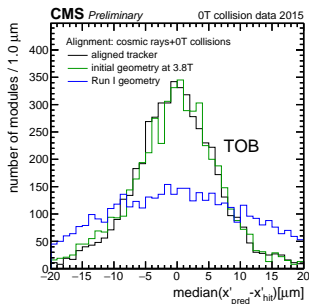
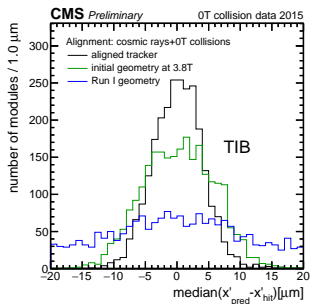
The distribution of median residuals is plotted for the local x - and y -directions in the barrel pixel detector, using 1.8 million collision tracks collected with the magnetic field turned off. The blue line shows the Run I geometry, which is no longer valid for Run II data, primarily because of temperature changes and pixel re-centering and repair. The green line shows the data refitted with the initial geometry used for data taking, which was determined using 0 T and 3.8 T cosmic ray data and which was valid for data collected with the magnetic field turned on. The black line shows the data refitted with the alignment for this data period, produced with the Millepede-II and HIP algorithms using 0 T collisions and cosmic ray data. This alignment recovers the changes in the tracker geometry between the two run periods, which are primarily a result of the change in the magnetic field. The RMS of the distribution reduces from 96.5 and 11.4 to 1.8 μm (x) and 71.2 and 24.7 to 7.4 μm (y) for the Run I, initial, and aligned geometry, respectively.

0 T Collision Data: FPIX



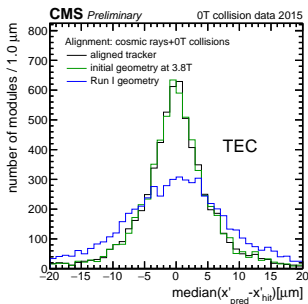
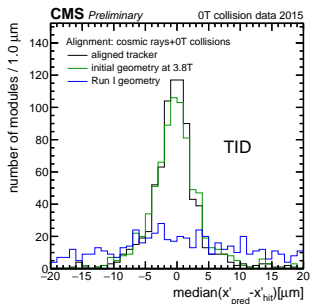
The distribution of median residuals is plotted for the local x - and y -directions in the forward pixel detectors, using 1.8 million collision tracks collected with the magnetic field turned off. The blue line shows the Run I geometry, which is no longer valid for Run II data, primarily because of temperature changes and pixel re-centering and repair. The green line shows the data refitted with the initial geometry used for data taking, which was determined using 0 T and 3.8 T cosmic ray data and which was valid for data collected with the magnetic field turned on. The black line shows the data refitted with the alignment for this data period, produced with the Millepede-II and HIP algorithms using 0 T collisions and cosmic ray data. This alignment recovers the changes in the tracker geometry between the two run periods, which are primarily a result of the change in the magnetic field. The RMS of the distribution reduces from 49.9 and 21.8 to 10.9 μm (x) and 27.9 and 25.2 to 14.0 μm (y) for the Run I, initial, and aligned geometry, respectively.

0 T Collision Data: TIB and TOB



The distribution of median residuals is plotted for the tracker inner and outer barrel, using 1.8 million collision tracks collected with the magnetic field turned off. The blue line shows the Run I geometry, which is no longer valid for Run II data, primarily because of temperature changes and pixel re-centering and repair (since tracks are fitted using hits in both the pixel and the strip detectors, the large movements of the pixel detectors also affect the DMR performance in the strip detectors). The green line shows the data refitted with the initial geometry used for data taking, which was determined using 0 T and 3.8 T cosmic ray data and which was valid for data collected with the magnetic field turned on. The black line shows the data refitted with the alignment for this data period, produced with the Millepede-II and HIP algorithms using 0 T collisions and cosmic ray data. This alignment recovers the changes in the tracker geometry between the two run periods, which are primarily a result of the change in the magnetic field. The RMS of the distribution reduces from 20.1 to 5.6 and 4.0 μm (TIB) and 17.8 to 7.7 and 7.4 μm (TOB) for the Run I, initial, and aligned geometry, respectively.

0 T Collision Data: TID and TEC

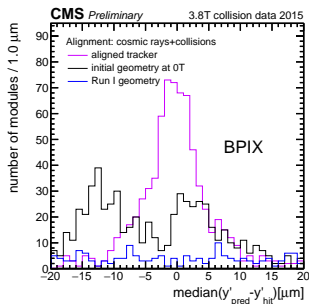
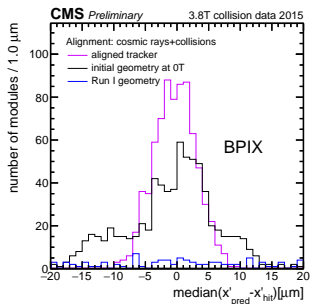


The distribution of median residuals is plotted for the tracker inner disks and endcaps, using 1.8 million collision tracks collected with the magnetic field turned off. The blue line shows the Run I geometry, which is no longer valid for Run II data, primarily because of temperature changes and pixel re-centering and repair (since tracks are fitted using hits in both the pixel and the strip detectors, the large movements of the pixel detectors also affect the DMR performance in the strip detectors). The green line shows the data refitted with the initial geometry used for data taking, which was determined using 0 T and 3.8 T cosmic ray data and which was valid for data collected with the magnetic field turned on. The black line shows the data refitted with the alignment for this data period, produced with the Millepede-II and HIP algorithms using 0 T collisions and cosmic ray data. The improvements from this alignment are mostly seen in the pixel modules, but also improve the strips to a lesser degree. The RMS of the distribution reduces from 22.1 to 4.5 μm (TID) and 13.5 to 7.0 μm (TEC) for the Run I and the initial and aligned geometry, respectively.

3.8 T Collision Data

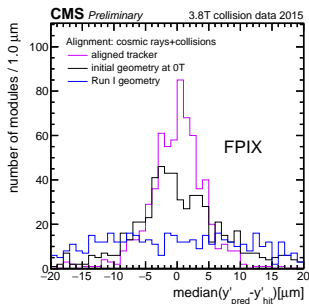
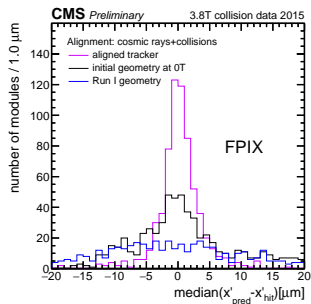
The tracker geometry changed again when the magnetic field was turned back on. This alignment was produced in an automated process, which will be used as part of the Prompt Calibration Loop (PCL), which activates as the data is collected and processed. Alignment is performed with a relatively small amount tracks (much less than the 20 million tracks used in the validation below), and the current alignment is used as a starting point. New alignment constants are fitted for larger substructures of the pixel detector (BPIX half-barrels and FPIX half-cylinders) only. The changes, again produced by the changing magnetic field, are recovered by this alignment.

3.8 T Collision Data: BPIX



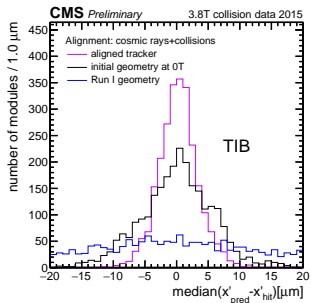
The distribution of median residuals is plotted for the local x - and y -directions in the barrel pixel detector, using 20 million collision tracks collected with the magnetic field at 3.8 T. The blue line shows the Run I geometry, which is no longer valid for Run II data, primarily because of temperature changes and pixel re-centering and repair. The black line shows the starting geometry for data taking, which was valid for data taken with the magnetic field turned off, as it was produced with the Millepede-II and HIP algorithms using cosmic ray and 0 T collision data. The alignment shown in violet was adjusted from this geometry by an automated alignment process of the pixel detector that will be run as part of the Prompt Calibration Loop as data is collected and processed, and shows improvements over the initial geometry. The changes resulted primarily from the change in the magnetic field. The RMS of the distribution reduces from 118.9 and 9.4 to 3.3 μm (x) and 90.1 and 27.0 to 10.0 μm (y) for the Run I, initial, and aligned geometry, respectively. The double-peak structure in y present when assuming the initial geometry in the track refit is corrected by the PCL-style alignment of the pixel detector.

3.8 T Collision Data: FPIX



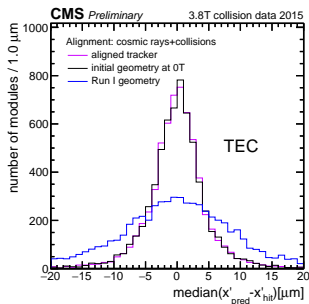
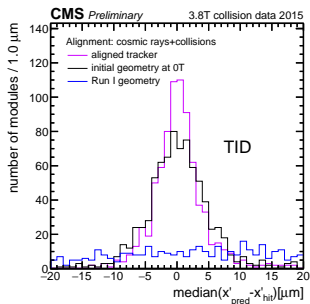
The distribution of median residuals is plotted for the local x - and y -directions in the forward pixel detector, using 20 million collision tracks collected with the magnetic field at 3.8 T. The blue line shows the Run I geometry, which is no longer valid for Run II data, primarily because of temperature changes and pixel re-centering and repair. The black line shows the starting geometry for data taking, which was valid for data taken with the magnetic field turned off, as it was produced with the Millepede-II and HIP algorithms using cosmic ray and 0 T collision data. The alignment shown in violet was adjusted from this geometry by an automated alignment process of the pixel detector that will be run as part of the Prompt Calibration Loop as data is collected and processed, and shows improvements over the initial geometry. The changes resulted primarily from the change in the magnetic field. The RMS of the distribution reduces from 63.1 and 13.6 to 4.6 μm (x) and 32.7 and 11.7 to 7.1 μm (y) for the Run I, initial, and aligned geometry, respectively.

3.8 T Collision Data: TIB



The distribution of median residuals is plotted for the tracker inner barrel, using 20 million collision tracks collected with the magnetic field at 3.8 T. The blue line shows the Run I geometry, which is no longer valid for Run II data, primarily because of temperature changes and pixel re-centering and repair (since tracks are fitted using hits in both the pixel and the strip detectors, the large movements of the pixel detectors also affect the DMR performance in the strip detectors). The black line shows the starting geometry for data taking, which was valid for data taken with the magnetic field turned off, as it was produced with the Millepede-II and HIP algorithms using cosmic ray and 0 T collision data. The alignment shown in violet was adjusted from this geometry by an automated alignment process of the pixel detector that will be run as part of the Prompt Calibration Loop as data is collected and processed, and shows improvements over the initial geometry. The changes resulted primarily from the change in the magnetic field. The RMS of the distribution reduces from 36.3 and 5.8 to 3.1 μm for the Run I, initial, and aligned geometry, respectively.

3.8 T Collision Data: TID and TEC

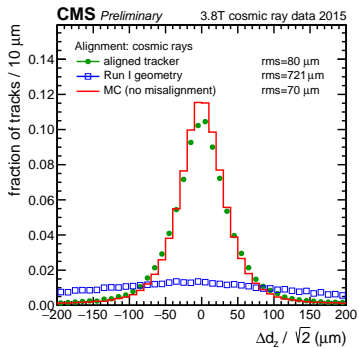
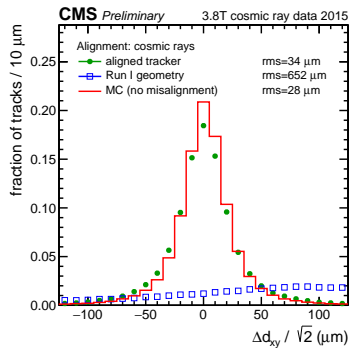


The distribution of median residuals is plotted for the tracker inner disks and endcaps, using 20 million collision tracks collected with the magnetic field at 3.8 T. The blue line shows the Run I geometry, which is no longer valid for Run II data, primarily because of temperature changes and pixel re-centering and repair (since tracks are fitted using hits in both the pixel and the strip detectors, the large movements of the pixel detectors also affect the DMR performance in the strip detectors). The black line shows the starting geometry for data taking, which was valid for data taken with the magnetic field turned off, as it was produced with the Millepede-II and HIP algorithms using cosmic ray and 0 T collision data. The alignment shown in violet was adjusted from this geometry by an automated alignment process of the pixel detector that will be run as part of the Prompt Calibration Loop as data is collected and processed, and shows improvements over the initial geometry. The changes resulted primarily from the change in the magnetic field, and affected the inner detectors more than the outer detectors such as the TEC. The RMS of the distribution reduces from 42.1 to 5.4 and 4.6 μm (TID) and 13.3 to 5.3 and 5.2 μm (TEC) for the Run I, initial, and aligned geometry, respectively.

Cosmic-Track Splitting Validation

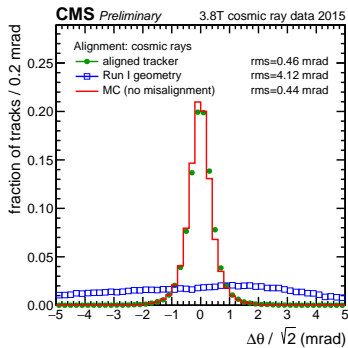
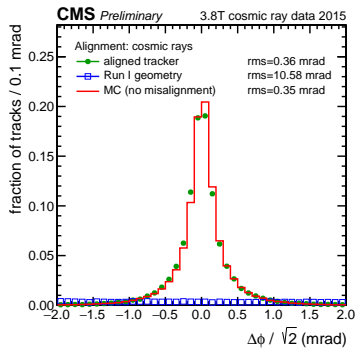
Cosmic ray tracks are split in half at the hit closest to origin and refitted with the alignment constants under consideration. The differences in various track parameters between the two half-tracks are studied. The width of the distribution measures the achieved alignment precision, while deviations from zero indicate possible biases.

3.8 T Cosmic-Ray Data: Δd_{xy} and Δd_z



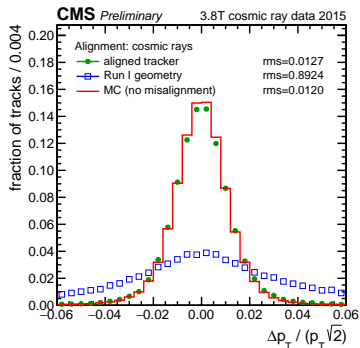
The normalized differences between two halves of a cosmic track, split at the point of closest approach to the interaction region, in d_{xy} , the xy distance, and d_z , the z distance, between the track and the origin. The observed precision using the aligned geometry (green circles), produced with the Millepede-II and HIP algorithms using cosmic ray data at 0 and 3.8 T, is a major improvement over the Run I geometry (blue empty squares) which is no longer valid for Run II data, primarily because of temperature changes and pixel re-centering and repair. The precision comes close to that of the ideal Monte Carlo, illustrating that the tracker has almost reached its design spatial resolution.

3.8 T Cosmic-Ray Data: Δd_ϕ and Δd_θ



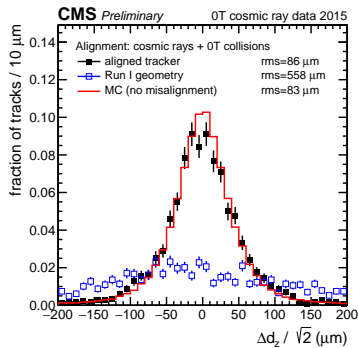
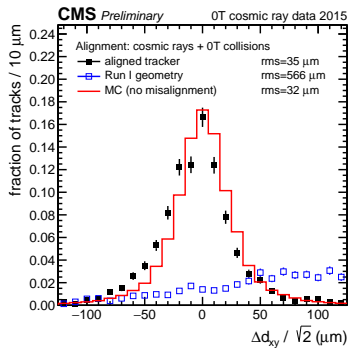
The normalized differences between two halves of a cosmic track, split at the point of closest approach to the interaction region, in the track's azimuthal angle ϕ and polar angle θ . The observed precision using the aligned geometry (green circles), produced with the Millepede-II and HIP algorithms using cosmic ray data at 0 and 3.8 T, is a major improvement over the Run I geometry (blue empty squares) which is no longer valid for Run II data, primarily because of temperature changes and pixel re-centering and repair. The precision comes close to that of the ideal Monte Carlo, illustrating that the tracker has almost reached its design angular resolution.

3.8 T Cosmic-Ray Data: Δp_T



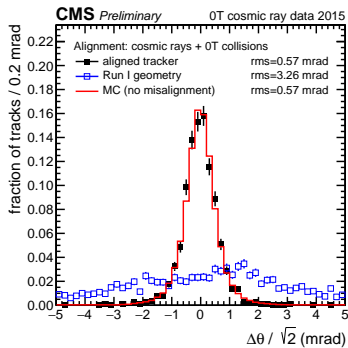
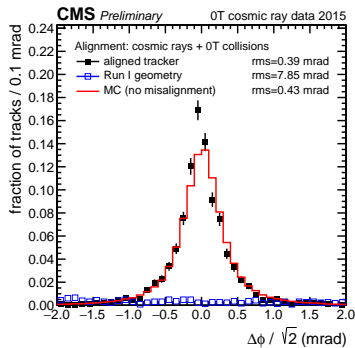
The normalized differences between two halves of a cosmic track, split at the point of closest approach to the interaction region, in the track's transverse momentum p_T . The observed precision using the aligned geometry (green circles), produced with the Millepede-II and HIP algorithms using cosmic ray data at 0 and 3.8 T, is a major improvement over the Run I geometry (blue empty squares) which is no longer valid for Run II data, primarily because of temperature changes and pixel re-centering and repair. The precision comes close to that of the ideal Monte Carlo, illustrating that the tracker has almost reached its design momentum resolution.

0 T Cosmic-Ray Data: Δd_{xy} and Δd_z



The normalized differences between two halves of a cosmic track, split at the point of closest approach to the interaction region, in d_{xy} , the xy distance, and d_z , the z distance, between the track and the origin. The observed precision using the aligned geometry (black filled squares), produced with the Millepede-II and HIP algorithms using cosmic ray and 0T collision data, is a major improvement over the Run I geometry (blue empty squares) which is no longer valid for Run II data, primarily because of temperature changes and pixel re-centering and repair. The precision comes close to that of the ideal Monte Carlo, illustrating that the tracker has almost reached its design spatial resolution.

0 T Cosmic-Ray Data: Δd_ϕ and Δd_θ



The normalized differences between two halves of a cosmic track, split at the point of closest approach to the interaction region, in the track's azimuthal angle ϕ and polar angle θ . The observed precision using the aligned geometry (black filled squares), produced with the Millepede-II and HIP algorithms using cosmic ray and 0 T collision data, is a major improvement over the Run I geometry (blue empty squares) which is no longer valid for Run II data, primarily because of temperature changes and pixel re-centering and repair. The precision is approximately the same as that of the ideal Monte Carlo, illustrating that the tracker has reached its design angular resolution for 0 tesla data. The small difference in Δd_ϕ is believed to be the result of a statistical fluctuation.

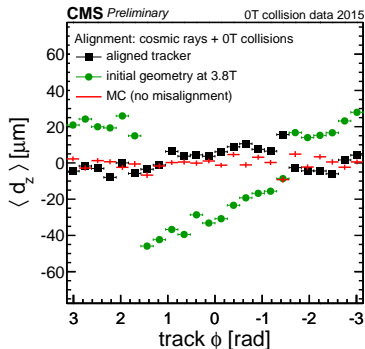
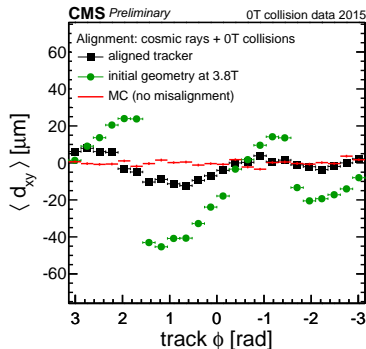
Primary-Vertex Validation

The resolution of the reconstructed vertex position is driven by the pixel detector since it is the closest detector to the interaction point and has the best hit resolution. The primary vertex residual method is based on the study the distance between the track and the vertex, the latter reconstructed without the track under scrutiny (unbiased track-vertex residual).

Selection and reconstruction of the events is as follows. Events used in this analysis are selected online with minimum bias triggers. The fit of the vertex must have at least 4 degrees of freedom. For each of the vertices, the impact parameters are measured for tracks with: more than 6 hits in the tracker, of which at least two are in the pixel detector; at least one hit in the first layer of the BPIX or the first disk of the FPIX; and χ^2/ndof of the track fit < 5 . The vertex position is recalculated excluding the track under scrutiny. A deterministic annealing clustering algorithm [3] is used in order to make the method robust against pileup, as in the default reconstruction sequence.

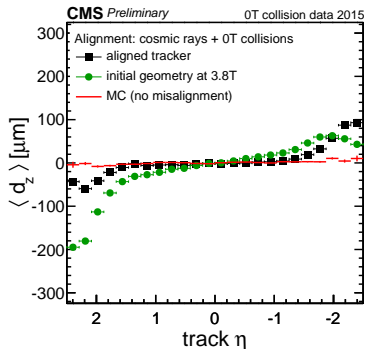
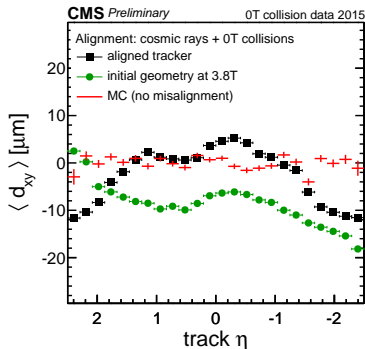
The distributions of the unbiased track-vertex residuals in the transverse plane, d_{xy} , and in the longitudinal direction, d_z , are studied in bins of track azimuth ϕ and pseudo-rapidity η . Random misalignments of the modules affect only the resolution of the unbiased track-vertex residual, increasing the width of the distributions, but without biasing their mean. Systematic movements of the modules will bias the distributions in a way that depends on the nature and size of the misalignment and the and of the selected tracks.

Primary-Vertex Validation: d_{xy} and d_z vs ϕ



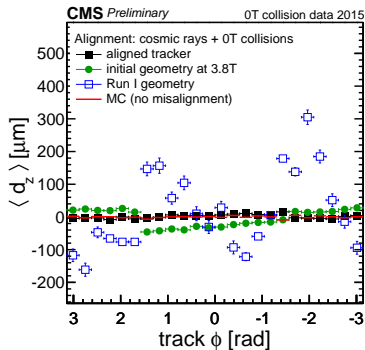
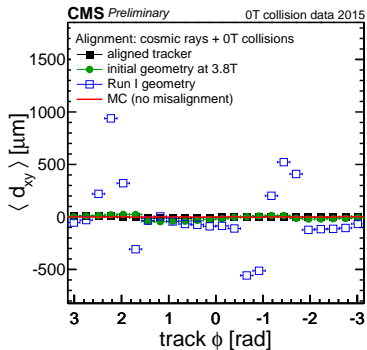
The distance in the transverse (d_{xy}) and longitudinal (d_z) plane of the track at its closest approach to a refit unbiased primary vertex is studied in bins of track azimuth ϕ using a sample of around 5.5M events collected by the CMS detector at zero magnetic field (0 T) selected online through minimum bias triggers. The performance of a dedicated alignment achieved with the Millepede-II and HIP algorithms using cosmic ray data collected with 0 T and 3.8 T magnetic field and 0 T collision data is compared to the one of a previous alignment reached during the commissioning phase with cosmic ray tracks at full magnetic field and to a detailed detector simulation with perfect alignment and calibration. The structures of the green curve indicate relative movements of the BPIX half-barrels.

Primary-Vertex Validation: d_{xy} and d_z vs η



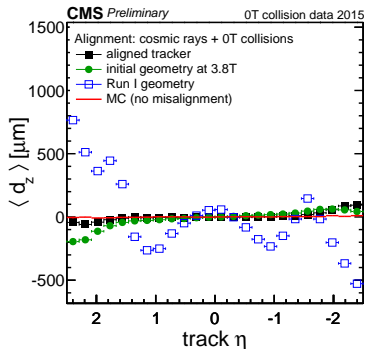
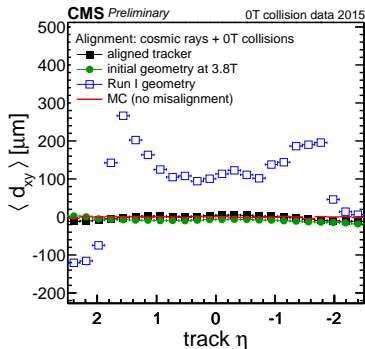
The distance in the transverse (d_{xy}) and longitudinal (d_z) plane of the track at its closest approach to a refit unbiased primary vertex is studied in bins of track pseudo-rapidity η using a sample of around 5.5M events collected by the CMS detector at zero magnetic field (0 T) selected online through minimum bias triggers. The performance of a dedicated alignment achieved with the Millepede-II and HIP algorithms using cosmic ray data collected with 0 T and 3.8 T magnetic field and 0 T collision data is compared to the one of a previous alignment reached during the commissioning phase with cosmic ray tracks at full magnetic field and to a detailed detector simulation with perfect alignment and calibration. Non optimal performance in the high pseudo-rapidity bins is understood in term of not yet perfect alignment of the FPIX modules, due to low illumination of this part of the detector to cosmic rays and to the limited amount of collision tracks used in the alignment fit.

Primary-Vertex Validation: d_{xy} and d_z vs ϕ






The distance in the transverse (d_{xy}) and longitudinal (d_z) plane of the track at its closest approach to a refit unbiased primary vertex is studied in bins of track azimuth ϕ using a sample of around 5.5M events collected by the CMS detector at zero magnetic field (0 T) selected online through minimum bias triggers. The performance of a dedicated alignment achieved with the Millepede-II and HIP algorithms using 0 T and 3.8 T cosmic ray and 0 T collision data is compared to the one of a previous alignment reached during the commissioning phase with cosmic ray tracks at full magnetic field, to the alignment used during end of Run I, and to a detailed detector simulation with perfect alignment and calibration. Large biases in the Run I geometry are expected due to the shifts (-1.3,-3.38) mm introduced in (x,y) in the re-centering procedure of the BPIX around the beampipe during the installation phase.

Primary-Vertex Validation: d_{xy} and d_z vs η



The distance in the transverse (d_{xy}) and longitudinal (d_z) plane of the track at its closest approach to a refit unbiased primary vertex is studied in bins of track pseudo-rapidity η using a sample of around 5.5M events collected by the CMS detector at zero magnetic field (0 T) selected online through minimum bias triggers. The performance of a dedicated alignment achieved with the Millepede-II and HIP algorithms using 0 T and 3.8 T cosmic ray and 0 T collision data is compared to the one of a previous alignment reached during the commissioning phase with cosmic ray tracks at full magnetic field, to the alignment used at the end of Run I and to a detailed detector simulation with perfect alignment and calibration. Large biases in the Run I geometry are expected due to the shifts $(-1.3, -3.38)$ mm introduced in (x, y) in the re-centering procedure of the BPIX around the beampipe during the installation phase. The structures at large absolute η ; are attributed to systematic effects still present in the FPIX, which require more 3.8 T collision data to be corrected by the alignment.

References

-  CMS Collaboration, “Alignment of the CMS tracker with LHC and cosmic ray data”, *JINST* **9** (2014) P06009, doi:10.1088/1748-0221/9/06/P06009
-  CMS Collaboration, “Alignment of the CMS silicon tracker during commissioning with cosmic rays” *JINST* **5** (2010) T03009, doi:10.1088/1748-0221/5/03/T03009
-  CMS Collaboration, “Description and performance of track and primary-vertex reconstruction with the CMS tracker”, *JINST* **9** (2014) P10009, doi:10.1088/1748-0221/9/10/P10009